

REPORT DOCUMENTATION PAGE

Form Approved
OMB No. 0704-0188

Public reporting burden for this collection of information is estimated to average 1 hour per response, including the time for reviewing instructions, searching existing data sources, gathering and maintaining the data needed, and completing and reviewing this collection of information. Send comments regarding this burden estimate or any other aspect of this collection of information, including suggestions for reducing this burden to Department of Defense, Washington Headquarters Services, Directorate for Information Operations and Reports (0704-0188), 1215 Jefferson Davis Highway, Suite 1204, Arlington, VA 22202-4302. Respondents should be aware that notwithstanding any other provision of law, no person shall be subject to any penalty for failing to comply with a collection of information if it does not display a currently valid OMB control number. **PLEASE DO NOT RETURN YOUR FORM TO THE ABOVE ADDRESS.**

1. REPORT DATE (DD-MM-YYYY) 03-05-2011		2. REPORT TYPE		3. DATES COVERED (From - To)	
4. TITLE AND SUBTITLE High-Order CESE Methods for Solving Hyperbolic PDEs (Preprint)				5a. CONTRACT NUMBER	
				5b. GRANT NUMBER	
				5c. PROGRAM ELEMENT NUMBER	
6. AUTHOR(S) David L. Bilyeu, Yung-Yu Chen, S.-T. John Yu, and Jean-Luc Cambier				5d. PROJECT NUMBER	
				5f. WORK UNIT NUMBER 23041057	
7. PERFORMING ORGANIZATION NAME(S) AND ADDRESS(ES) Air Force Research Laboratory (AFMC) AFRL/RZSS 1 Ara Road Edwards AFB CA 93524-7013				8. PERFORMING ORGANIZATION REPORT NUMBER AFRL-RZ-ED-JA-2011-151	
9. SPONSORING / MONITORING AGENCY NAME(S) AND ADDRESS(ES) Air Force Research Laboratory (AFMC) AFRL/RZS 5 Pollux Drive Edwards AFB CA 93524-7048				10. SPONSOR/MONITOR'S ACRONYM(S)	
				11. SPONSOR/MONITOR'S NUMBER(S) AFRL-RZ-ED-JA-2011-151	
12. DISTRIBUTION / AVAILABILITY STATEMENT Approved for public release; distribution unlimited (PA #11209).					
13. SUPPLEMENTARY NOTES For publication in the International Journal of Computational Fluid Dynamics					
14. ABSTRACT In the present paper, we extend Chang's (Chang (2010)) high-order method for system of linear and non-linear hyperbolic partial differential equations. A general formulation is presented for solving the coupled equations with arbitrarily high-order accuracy. To demonstrate the formulation, several linear and non-linear cases are reported. First, we solve a convection equation with source term and the linear acoustics equations. We then solve the Euler equations for acoustic waves, a blast wave, and Shu and Osher's test case for acoustic waves interacting with a shock. Numerical results show higher-order convergence by continuous mesh refinement. The new high-order CESE method shares many favorable attributes of the original second-order CESE method, including: (i) compact mesh stencil involving only the immediate mesh nodes surrounding the node where the solution is sought, (ii) the CFL stability constraint remains to be the same, i.e., ≤ 1 , as compared to the original second-order method, and (iii) shock capturing capability without using an approximate Riemann solver.					
15. SUBJECT TERMS					
16. SECURITY CLASSIFICATION OF:			17. LIMITATION OF ABSTRACT	18. NUMBER OF PAGES	19a. NAME OF RESPONSIBLE PERSON
a. REPORT	b. ABSTRACT	c. THIS PAGE			Dr. Jean-Luc J. Cambier
Unclassified	Unclassified	Unclassified	SAR	21	19b. TELEPHONE NUMBER (include area code) N/A

RESEARCH ARTICLE

High-Order CESE Methods for Solving Hyperbolic PDEs

David L. Bilyeu^{*a,b}, Yung-Yu Chen^a, S.-T. John Yu^{*a} and Jean-Luc Cambier^b

^a*The Ohio State University, Columbus, OH 43210, USA;* ^b*Air Force Research Lab,
 Edwards AFB, CA 93524, USA*

(Received 00 Month 200x; final version received 00 Month 200x)

In the present paper, we extend Chang's (Chang (2010)) high-order method for system of linear and non-linear hyperbolic partial differential equations. A general formulation is presented for solving the coupled equations with arbitrarily high-order accuracy. To demonstrate the formulation, several linear and non-linear cases are reported. First, we solve a convection equation with source term and the linear acoustics equations. We then solve the Euler equations for acoustic waves, a blast wave, and Shu and Osher's test case for acoustic waves interacting with a shock. Numerical results show higher-order convergence by continuous mesh refinement. The new high-order CESE method shares many favourable attributes of the original second-order CESE method, including: (i) compact mesh stencil involving only the immediate mesh nodes surrounding the node where the solution is sought, (ii) the CFL stability constraint remains to be the same, i.e., ≤ 1 , as compared to the original second-order method, and (iii) shock capturing capability without using an approximate Riemann solver.

Keywords: CESE; Higher Order; Arbitrary Order; CFD; Euler Equation; Acoustic Equation

1. Introduction

In this work, we extend Chang's fourth-order CESE method (Chang (2010)) for a single non-linear hyperbolic equation to a system of coupled hyperbolic partial differential equations (PDEs). The new formulation is general and can be used to achieve an arbitrarily order of convergence. To demonstrate the capabilities of the new scheme, we apply the method to solve three sets of equations: (i) the one-dimensional Euler equations, (ii) the linearised acoustic equations, and (iii) a convection equation with a source term.

The original second-order CESE method of (Chang (1995)) solves the hyperbolic PDEs by discretizing the space-time domain by using the conservation elements (CEs) and solution elements (SEs). The profiles of unknowns are prescribed by assumed discretization

*Corresponding Author. Email: bilyeu.4@osu.edu

inside SEs. Aided by the approximation for the unknowns in the SEs, space-time flux conservation can be enforced over each CE. The calculation of space-time flux conservation results in the formulation for updating the unknowns in the time marching process. The special features of the CESE method include: (i) The a scheme, the core scheme of the CESE method, is non-dissipative. (ii) The CESE method has the most compact mesh stencil possible, involving only the immediate neighbouring mesh points that surround the node where the solution is sought. (iii) The method uses explicit integration in time marching. The stability criterion is $CFL \leq 1$. (iv) No Riemann solver is used and the scheme is simple and efficient. The CESE scheme has been previously used to solve a multitude of different physics in one, two and three dimensions, including: MHD (Zhang *et al.* (2006)), Navier-Stokes (Zhang *et al.* (2000), Chang (2007), Venkatachari *et al.* (2008)), waves in solids, (Chen *et al.* (2011), Yang *et al.* (2011)).

This paper is organized as the following. Section 2 reports the fourth-order CESE method for the coupled equations formulated in a vector form. Section 3.3 shows the application of the general formulation to the one-dimensional Euler, linear acoustic, and convection equation. Section 3 provides the results and discussions and our conclusion in section 4.

2. Arbitrary-Order, One-Dimensional CESE Method

Consider a system of coupled convection equations:

$$\frac{\partial \mathbf{U}}{\partial t} + \frac{\partial \mathbf{F}}{\partial x} = \mathbf{S}, \quad (1)$$

where

$$\mathbf{U} \stackrel{\text{def}}{=} (u_1, u_2, u_3, \dots, u_M)^T, \text{ - conserved variables}$$

$$\mathbf{F} \stackrel{\text{def}}{=} (f_1, f_2, f_3, \dots, f_M)^T, \text{ - fluxes}$$

$$\mathbf{S} \stackrel{\text{def}}{=} (s_1, s_2, s_3, \dots, s_M)^T, \text{ - source terms}$$

There are M equations to be solved in the system Eq. (1).

The space-time stencil used in this derivation is the same as that reported by Chang (Chang and Wang (2003)) and is repeated here for completeness. In Fig. (1) the solid dots A , C , and E are the solution points. A is at (x_j, t^n) and C and E are at $(x_{j-1/2}, t^{n-1/2})$ and $(x_{j+1/2}, t^{n-1/2})$, respectively. P^+ is between M^+ and F . P^- is between M^- and B . The distance between P^\pm and M^\pm is determined by a parameter τ . The rectangles $ABCD$ and $ADEF$ are basic CEs (BCEs), while the rectangle $BCEF$ is the compound CE (CCE) associated with the solution point A .

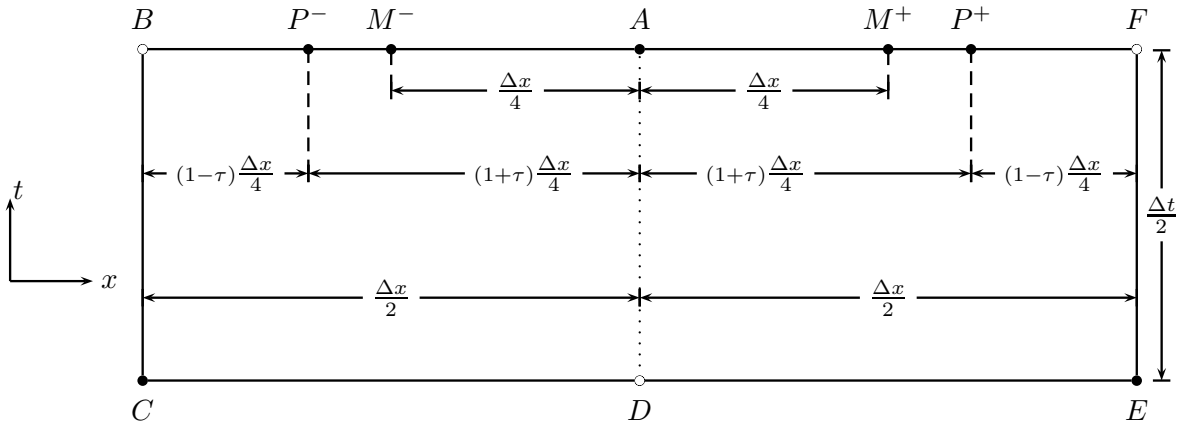


Figure 1.: Mesh nodes in the one-dimensional CESE methods.

To facilitate the discussion, we let $SE(j, n)$ denotes the SE located at $x = x_j$ and $t = t^n$. To denote high-order derivatives, we use the following notations:

$$u_{mx^a t^b} = \frac{\partial^{a+b} u_m}{\partial x^a \partial t^b}$$

In $SE(j, n)$, the unknown variables u_m , $m = 1, \dots, M$, are approximated by a Taylor series:

$$u_m^*(x, t; j, n) \stackrel{\text{def}}{=} \sum_{a=0}^{N_M} \sum_{b=0}^{N_M-a} \frac{(u_{mx^a t^b})_j^n}{a!b!} (x - x_j)^a (t - t^n)^b, \quad (2)$$

where N_M is the desired order subtracted by 1, e.g., for the fourth-order scheme, $N_M = 3$. The superscript * represents the numerical approximation of the variable. Inside of a SE $u_{mx^a t^b}$ are constant. The flux functions f_m , $m = 1, \dots, M$, can also be represented with the Taylor expansion as:

$$f_m^*(x, t; j, n) \stackrel{\text{def}}{=} \sum_{a=0}^{N_M} \sum_{b=0}^{N_M-a} \frac{(f_{mx^a t^b})_j^n}{a!b!} (x - x_j)^a (t - t^n)^b. \quad (3)$$

Inside a SE, $f_{mx^a t^b}$ are constant. An advantage of a Taylor series is that its derivatives can also be expressed as a Taylor series

$$u_{mx^z t^i}^*(x, t; j, n) = \sum_{a=0}^A \sum_{b=0}^{B-a} \frac{(u_{mx^{a+z} t^{b+i}})_j^n}{a!b!} (x - x_j)^a (t - t^n)^b; \quad \begin{matrix} A=N_M-z \\ B=N_M-z-i \end{matrix} \quad (4)$$

and

$$f_{mx^z t^i}^*(x, t; j, n) = \sum_{a=0}^A \sum_{b=0}^{B-a} \frac{(f_{mx^{a+z} t^{b+i}})_j^n}{a!b!} (x - x_j)^a (t - t^n)^b; \quad \begin{matrix} A=N_M-z \\ B=N_M-z-i \end{matrix}. \quad (5)$$

Equations 2 and 3 contain $2 \sum_{n=1}^{N_M+1} n$ unknowns. In the following derivation, it will be shown, that for a given $SE(j, n)$, the only independent variables are the spatial derivatives $(u_m)_j^n$, $(u_{mx})_j^n$, \dots , $(u_{mx^{N_M}})_j^n$, $m = 1, \dots, M$.

To proceed, for each $m = 1, \dots, M$, the unknowns are categorized as: (i) even-order derivatives, $(u_m)_j^n, (u_{mxx})_j^n, \dots, u_{mx^{2n}}$ and (ii) odd-order derivatives, $(u_{mx})_j^n, (u_{mxxx})_j^n, \dots, u_{mx^{2n+1}}$ $n = (OD - 1)/2$. Where OD is the accuracy of the Taylor series. In what follows, we introduce an arbitrary order CESE $c-\tau$ scheme for a system of M PDEs. The $c-\tau$ scheme uses space-time integration for the advancing formula for the even-order derivatives, while the odd-order derivatives are calculated from a central-difference-like procedure.

2.1. Even-Order Derivatives

It can be shown that by differentiating Eq. (8) twice with respect to x , we obtain:

$$\frac{\partial u_{mxx}^*(x, t; j, n)}{\partial t} + \frac{\partial f_{mxx}^*(x, t; j, n)}{\partial x} = \frac{\partial^2 s_m^*}{\partial x^2}, \quad m = 1, \dots, M, \quad (10)$$

or in a more general form

$$\frac{\partial u_{mx^{2z}}^*(x, t; j, n)}{\partial t} + \frac{\partial f_{mx^{2z}}^*(x, t; j, n)}{\partial x} = \frac{\partial^{2z} s_m^*}{\partial x^{2z}}, \quad z = 0, 1, \dots, (N_M - 1)/2. \quad (11)$$

Consider the Euclidean space \mathcal{E}^2 with the coordinates $(\xi_1, \xi_2) = (x, t)$. Aided by defining:

$$\mathbf{h}_{mx^{2z}}^* \stackrel{\text{def}}{=} (f_{mx^{2z}}^*(x, t; j, n), u_{mx^{2z}}^*(x, t; j, n))^T, \quad z = 1, \dots, (N_M - 1)/2,$$

and the divergence theorem, Eqs. (8) and (11) can be transformed into integral equations as:

$$\oint_{S(V)} \mathbf{h}_{mx^{2z}}^* \cdot d\mathbf{s} = s_{mx^{2z}}^*, \quad z = 0, \dots, (N_M - 1)/2, \quad (12)$$

where $S(V)$ is the closed boundary of an arbitrary region V and $d\mathbf{s}$ is defined in Fig. (2).

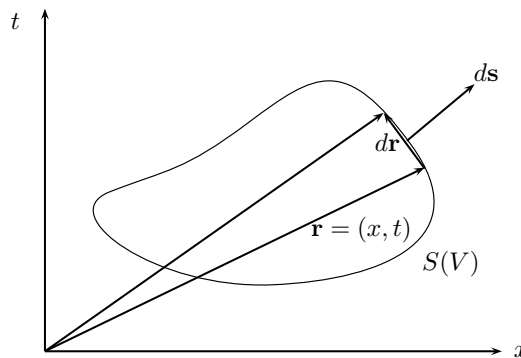


Figure 2.: Space-time integration over an arbitrary closed domain V .

We define:

$$u_{m\bar{x}z\bar{t}^k}^* \stackrel{\text{def}}{=} \frac{\partial^{z+k} u_m^*}{\partial x^z t^k} \left(\frac{\Delta x}{4} \right)^z \left(\frac{\Delta t}{4} \right)^k \quad (13)$$

$$f_{m\bar{x}z\bar{t}^k}^* \stackrel{\text{def}}{=} \frac{\partial^{z+k} f_m^*}{\partial x^z t^k} \left(\frac{\Delta x}{4} \right)^z \left(\frac{\Delta t}{4} \right)^k \quad (14)$$

$$s_{m\bar{x}z\bar{t}^k} \stackrel{\text{def}}{=} \frac{\partial^{z+k} s_m}{\partial x^z t^k} \left(\frac{\Delta x}{4} \right)^z \left(\frac{\Delta t}{4} \right)^k \quad (15)$$

where $\Delta x = x_{j+1/2} - x_{j-1/2}$ and $\Delta t = t^n - t^{n-1}$. In order to write equations more compactly, any local constant enclosed within a square bracket will be evaluated at the location specified by the subscript and superscript written on the enclosing square bracket, e.g.:

$$(u_{mxx})_j^n + (u_{mxxx})_j^n \frac{\Delta x}{2} + (u_{mxxxt})_j^n \frac{\Delta t}{2} \equiv \left[u_{mxx} + u_{mxxx} \frac{\Delta x}{2} + u_{mxxxt} \frac{\Delta t}{2} \right]_j^n.$$

Aided by Eqs. (13) and (14), Eq. (12) gives:

$$\begin{aligned} (u_{m\bar{x}z})_j^n &= \frac{1}{\Delta x} \iint s_{m\bar{x}z} dV + \\ &\frac{1}{2} \sum_{k=0}^{N_M-z} \frac{2^k}{(k+1)!} \left(\left[u_{m\bar{x}^{k+z}} + \frac{\Delta t}{\Delta x} f_{m\bar{x}z\bar{t}^k} \right]_{j-1/2}^{n-1/2} + \left[(-1)^k u_{m\bar{x}^{k+z}} - \frac{\Delta t}{\Delta x} f_{m\bar{x}z\bar{t}^k} \right]_{j+1/2}^{n-1/2} \right) - \\ &\sum_{k=1}^{\frac{N_M-z-1}{2}} \frac{2^{2k}}{(2k+1)!} (u_{m\bar{x}^{2k+z}})_j^n \end{aligned} \quad (16)$$

Equation (16) provides an explicit formulation for all even spatial derivatives. As long as the highest even derivative is calculated first the last term on the RHS will have already been calculated. For example, in a fourth order accurate scheme the conserved variables are u_m, u_{mx}, u_{mx^2} , and u_{mx^3} . In this case $(u_{mx^2})_j^n$ will be calculated first followed by $(u_m)_j^n$. It should also be noted that the $*$ is absent from the source term. This is because the source term treatment varies when dealing with different flow physics and may not require a Taylor series expansion.

2.2. Odd-Order Derivatives

In order to compute the odd derivatives a central differencing approach is applied following the c - τ scheme. There are two possible formulations for the odd-order derivatives (i) the standard c - τ scheme which is applicable if there are no discontinuities present and (ii) a re-weighted c - τ minmod scheme which is used if there are discontinuities in the flow field.

In order to mitigate the dissipation as the local CFL number decreases the central differencing is applied at points P^+ and P^- , where P^\pm are points located at

$$x(P^+) = x_j + (1 + \tau) \frac{\Delta x}{4} = x_{j+1/2} - (1 - \tau) \frac{\Delta x}{4}, \quad (17)$$

$$x(P^-) = x_j - (1 + \tau) \frac{\Delta x}{4} = x_{j-1/2} + (1 - \tau) \frac{\Delta x}{4}. \quad (18)$$

Where τ is the absolute value of the local CFL number.

First we define $u_{m\bar{x}z}^*(P^\pm)$ to be the Taylor series expansion of $(u_{m\bar{x}z})_n^j$ from (x_j, t^n) to $x(P^\pm)$. Then we can solve for $u_{m\bar{x}z+1}$ by subtracting $u_{m\bar{x}z}^*(P^-)$ from $u_{m\bar{x}z}^*(P^+)$:

$$u_{m\bar{x}z+1} = \frac{u_{m\bar{x}z}^*(P^+) - u_{m\bar{x}z}^*(P^-)}{2(1 + \tau)} - \sum_{k=1}^{\frac{N_M-1-z}{2}} \frac{1}{(2k+1)!} u_{m\bar{x}2k+1+z} (1 + \tau)^{2k}, \quad (19)$$

for $z = 0, 2, 4, \dots, N_M - 1$ and $m = 1, 2, \dots, M$. Since we can not calculate $u_{m\bar{x}z}^*(P^\pm)$ we approximate it by $u'_{m\bar{x}z}(P^\pm)$. Where $u'_{m\bar{x}z}(P^\pm)$ is the Taylor series expansion from $(x_{j\pm 1/2}, t^{n-1/2})$ to $x(P^\pm)$ respectively.

$$u_{m\bar{x}z+1} = \frac{u'_{m\bar{x}z}(P^+) - u'_{m\bar{x}z}(P^-)}{2(1 + \tau)} - \sum_{k=1}^{\frac{N_M-1-z}{2}} \frac{1}{(2k+1)!} u_{m\bar{x}2k+1+z} (1 + \tau)^{2k},$$

When discontinuities are present in the flow field a re-weighting and or limiting of the derivatives is required. To calculate the odd derivatives we first apply re-weighting then check for smoothness. If the results are not found to be smooth we then apply a limiter such as the minmod operator to limit the derivatives.

To begin we outline the re-weighting algorithm. It should be noted that all previously re-weighting schemes used in second order CESE schemes should be applicable to the higher order CESE schemes. In this paper the derivation of the W2 scheme (Chang and Wang (2003)) will be presented. First the function W is given as

$$W_\pm(x_-, x_+, \alpha) = \frac{|x_\mp|^\alpha}{|x_-|^\alpha + |x_+|^\alpha}. \quad (20)$$

To remain stable in the presence of discontinuities $\alpha \geq 1$. The odd-order derivatives are now defined by:

$$(u_{m\bar{x}z})_j^n \stackrel{\text{def}}{=} (\omega_{m-})_z (\hat{u}_{m\bar{x}-z}) + (\omega_{m+})_z (\hat{u}_{m\bar{x}+z}), \quad (21)$$

where

$$(\omega_{m\pm})_z = W_\pm(u_{m\bar{x}-z}^c, u_{m\bar{x}+z}^c, \alpha_z), \quad (22)$$

with

$$\hat{u}_{m\bar{x}\mp z} \stackrel{\text{def}}{=} \pm \frac{(u_{m\bar{x}z-1})_j^n - u'_{m\bar{x}z-1}(P^\mp)}{1 + \tau},$$

$$u_{m\bar{x}z\mp}^c \stackrel{\text{def}}{=} \pm \frac{1}{2}((u_{m\bar{x}z-1})_j^n - (u'_{m\bar{x}z-1})_{j\mp 1/2}^n),$$

where $(u'_{m\bar{x}z-1})_{j\pm 1/2}^n$ is the Taylor series expansion from $(x_{j\pm 1/2}, n-1/2)$ to $(x_{j\pm 1/2}, n)$.

For solvers that are greater than 4th order it was found that the re-weighting scheme was not enough for stability. In this case we need to apply a limiter such as minmod when the solution is no longer smooth. We define a smoothness check as

$$\left| \frac{\partial^{k+1} u_m}{\partial \bar{x}^{k+1}} \right| > \left| \frac{4\beta}{k+1} \frac{\partial^k u_m}{\partial \bar{x}^k} \right| \text{ for } k > 1 \tag{23}$$

where β is an adjustable parameter on the order of 0.1 or 0.01. If Eq. (23) is found to be true then the minmod limiter was applied. This smoothness check was applied to all derivatives, even and odd, greater than 1. This test checks to make sure that each successive term in the Taylor series is a correction on the previous term.

The minmod operator is defined as

$$\text{minmod}(a, b) = \max(\min(1, a/b), 0). \tag{24}$$

So $u_{\bar{x}^k}$ is equal to

$$u_{\bar{x}^k} = \hat{u}_{m\bar{x}+k} \text{minmod}(\hat{u}_{m\bar{x}-k}, \hat{u}_{m\bar{x}+k}) \tag{25}$$

The above equations provide an explicit formulation for the odd spatial derivatives when discontinuities are present in the flow field.

2.3. Numerical Outline

To summarise the numerical procedure used is as follows:

- (1) First calculate all of the Taylor series coefficients for the flux and conserved variables at $(n - 1/2, j \pm 1/2)$, points *C* and *E* in Fig. 1. The flux and temporal derivative coefficients are calculated by Eqs. 7 and 8 respectively. It may also be necessary to calculate the source term coefficients.
- (2) Calculate all even derivatives using Eq. (16), starting with the highest unknown even derivative.
- (3) Calculate the highest odd derivative via Eq. (21)
- (4) Check for smoothness using Eq. (23) and apply minmod, Eq. (25), as needed
- (5) Repeat steps 3 and 4 until all odd derivatives are found
- (6) Check the even derivative for smoothness, Eq. (23), and apply the minmod, Eq. (25) limiter as needed. This is done for all even derivatives except the zero derivative, i.e. $k=0$ in Eq. (25).

3. Numerical Results

The following test cases show how the CESE method improves as the order of accuracy of the method employed increases. The test cases used for convergence tests are: (i) a simple convection equation with a source term, (ii) acoustic waves modelled by the linearised Euler equations, and (iii) acoustic waves modelled by the non-linear Euler equations. For all three cases, we calculate the order of accuracy by using the following formula:

$$\ell^2 \stackrel{\text{def}}{=} \sqrt{\int |\phi|^2 dx} \approx \sqrt{\sum_i |\phi_i|^2 \Delta x_i}$$

where ϕ_i is defined as the difference between the analytical and numerical solution and Δx_i is the grid spacing at a given location i . In all cases Δx is constant. The rate of convergence is taken as the slope of the best fit line through the points $(\log_{10}(\Delta x), \log_{10}(\ell^2))$.

3.1. Convection Equation with Source Term

The first test case is the convection equation with a source term. In this problem we solve

$$\begin{aligned} \frac{du}{dt} + a \frac{du}{dx} &= a S_0 \cos(x) \\ -2\pi < x < 2\pi; t > 0 \end{aligned}$$

where a and S_0 are constant. Under the periodic boundary condition the analytical solution to this problem is

$$u(x, t) = \cos(x - at) + S_0 \sin(x).$$

For this test case we need to integrate the source term. Since the source term is only dependent on x we can generate an analytical results equal to

$$\begin{aligned} \iint S &= a S_0 \frac{\Delta t}{2} \sin(x) \Big|_{x_{j-1/2}}^{x_{j+1/2}}, \\ \iint S_{\bar{x}\bar{x}} &= -a S_0 \left(\frac{\Delta x}{4}\right)^2 \frac{\Delta t}{2} \sin(x) \Big|_{x_{j-1/2}}^{x_{j+1/2}}, \dots, \\ \iint S_{\bar{x}^{2n}} &= (-1)^{n/2} a S_0 \left(\frac{\Delta x}{4}\right)^{2n} \frac{\Delta t}{2} \sin(x) \Big|_{x_{j-1/2}}^{x_{j+1/2}}, \text{ for } n = 0, 1, \dots, \frac{N_M - 1}{2}. \end{aligned}$$

For the convergence tests, $a = S_0 = 1$ and the test time was set to $2.5 \frac{l}{a}$, where l is the length of the domain. In all calculations, $\text{CFL} = 0.7$. Shown in Fig. (3) and Table (1), the actual convergence rate agrees well with the order of accuracy of the scheme employed. The computational scaling shows that by doubling the order of the Taylor series the time required to complete a simulation will increase by about $2^{2.2}$.

Table 1.: Convergence rates of the numerical solutions of the convection equation, and the averaged, normalized time for case with different order of accuracy.

Desired Order	Actual Order	Normalized Time
2	2.00	1.00
4	4.01	5.22
8	7.95	23.65
12	12.12	59.04
16	16.05	115.83
20	20.09	190.95

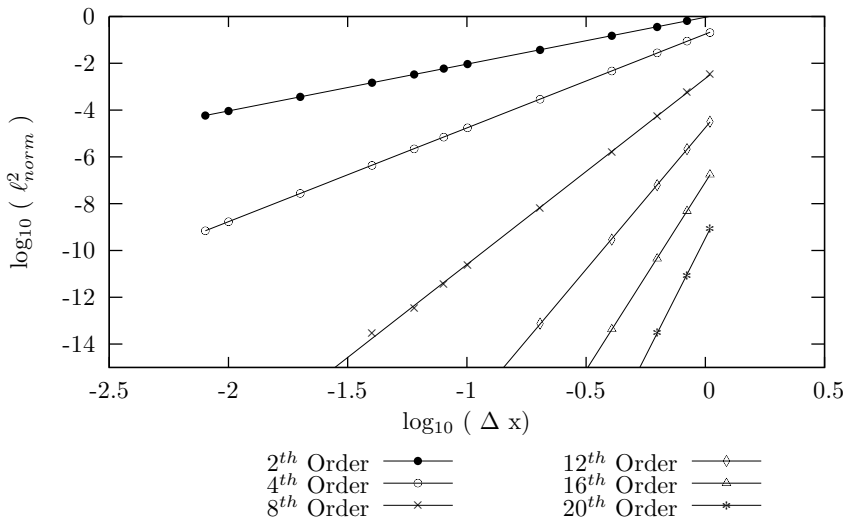


Figure 3.: The ℓ^2 norm of numerical solutions of the Convection equation with source term. The symbols represent the actual calculated data and the lines represent the best-fit curves of the data.

Another important aspect to consider is whether the higher-order resolution is worth the additional computational cost. For this, we refer to Fig. (4). Shown in the figures, it is more efficient to use a higher-order method rather than increasing the resolution for a linear solver.

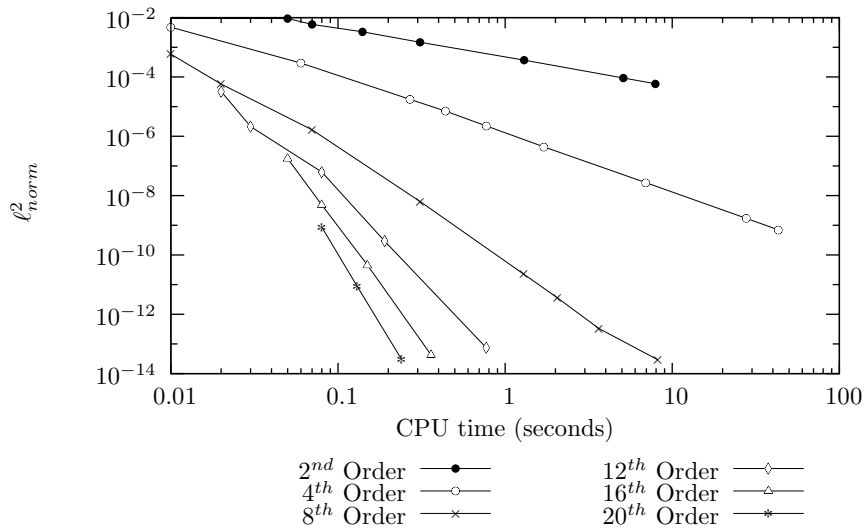


Figure 4.: The ℓ^2 norm versus the computational time for the solution of the convection equation.

3.2. Linear Acoustic Equation

The second test case is the acoustic wave solved by solving the linearised Euler equations. The conserved and flux values are

$$\mathbf{U} = (u_1, u_2)^T = (\rho, v)^T,$$

$$\mathbf{F} = \left(\rho_\infty v, \frac{a_\infty^2}{\rho_\infty} \rho \right)^T = \left(\rho_\infty u_2, \frac{a_\infty^2}{\rho_\infty} u_1 \right)^T$$

where ρ , U , and a are respectively the density, velocity, speed of sound. The speed of sound is equal to $\sqrt{\gamma p / \rho}$ with $\gamma=1.4$. The values with a subscript ∞ are mean values of the flow variables. The first-order derivatives for the flux functions are:

$$f_{11} = 0, f_{12} = \rho_\infty$$

$$f_{21} = \frac{a_\infty^2}{\rho_\infty}, f_{22} = 0.$$

Since all of the first-order derivatives are constant the higher derivatives are zero. This reduces the calculation of all fluxes to a matrix vector multiplication.

Under periodic boundary conditions the analytical solution for the linearised acoustic wave equation is

$$\rho = \rho_\infty + \frac{\varepsilon \rho_\infty}{a_\infty} \cos \left(\frac{2n\pi}{l} (x - a_\infty t) \right)$$

$$U = U_\infty + \varepsilon \cos \left(\frac{2n\pi}{l} (x - a_\infty t) \right)$$

$$\text{for } \frac{-l}{2} < x < \frac{l}{2}; t > 0$$

where n , l , and ε are respectively the number of waves in the domain, length of the

domain, and an amplification factor. For this test case $p_\infty=1$, $\rho_\infty=\gamma$, $\varepsilon=10^{-2}$, $n=1$, and $l=2$. The run time was equal to $4.25\frac{l}{a_\infty}$ which allows the wave to propagate through the domain 4.25 times. The CFL number is constant throughout the domain and is equal to 0.75. As seen in Fig. (5) our desired order of convergence closely matches the actual order of convergence. Table (2) shows the desired order of convergence, the actual order of convergence, and the normalized time. Figure 6 shows that it is typically more efficient to use a higher order scheme then to use more points. When the ℓ^2 norm is still relatively high, $OD(10^{-8})$ it was found that 8ththrough 20thorder schemes had approximately the same computational efficiency. The relative numerical cost was calculated by taking the average simulation time per cell per iteration for multiple resolutions and dividing it by the cost of the 2nd order version. The computational scaling shows that by doubling the order of the Taylor series the time required to complete a simulation will increase by about $2^{2.2}$.

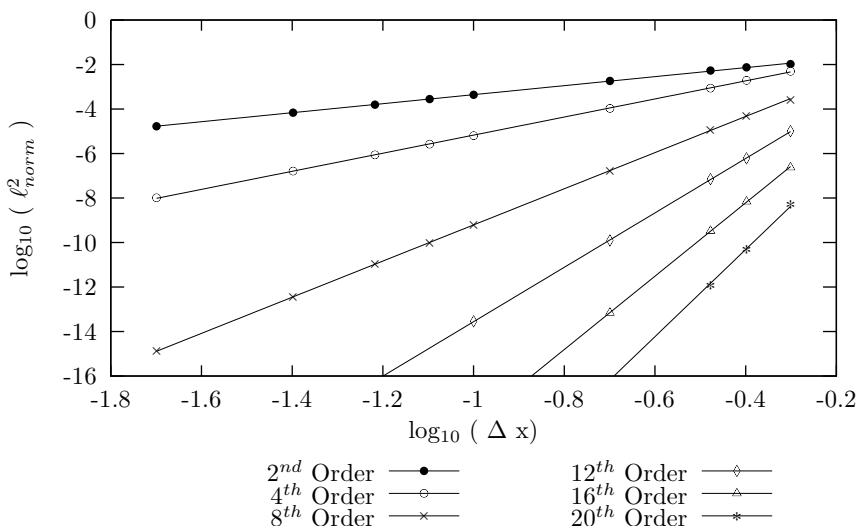


Figure 5.: The ℓ^2 norm of numerical solutions where points are actual calculated data and the line is a best-fit curve of the data.

Table 2.: Convergence rates for the linear acoustic solver and the average normalized time for case.

Desired Order	Actual Order	Normalized Time
2	2.03	1.00
4	4.06	3.43
8	8.12	14.47
12	12.21	34.33
16	16.48	67.98
20	20.52	116.89

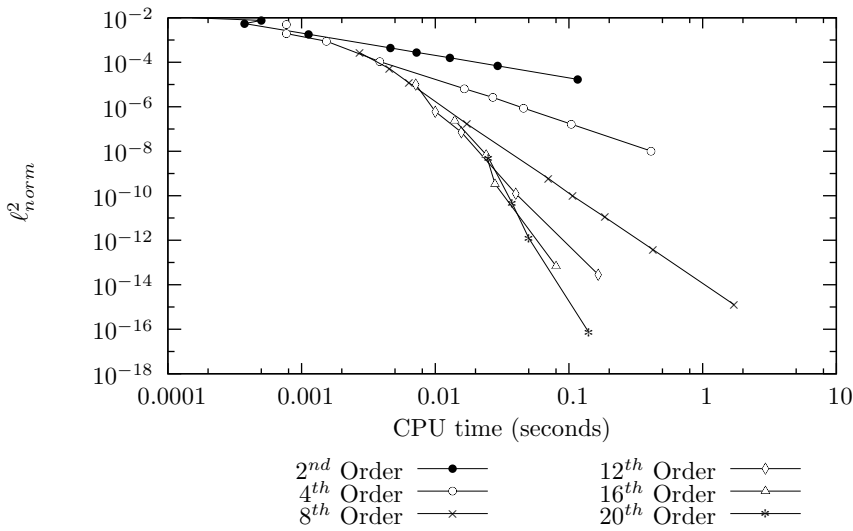


Figure 6.: The ℓ^2 norm versus the computational time for the solutions of the linear acoustic wave equations.

The above cases showed that we were able to achieve higher-order convergence for coupled, linear, wave equations.

3.3. Euler Equation

In this section we demonstrate higher order convergence test as well as our schemes ability to capture discontinuities.

To construct an arbitrary order CESE solver for the one-dimensional Euler equations, we plug the following unknown vector and flux function vector into Eq. (1):

$$\begin{aligned} \mathbf{U} &= (u_1, u_2, u_3)^T = (\rho, \rho v, p/(\gamma - 1) + \rho v^2/2)^T, \\ \mathbf{F} &= (\rho v, \rho v^2 + p, (\rho E + p)v)^T \\ &= (u_2, (\gamma - 1)u_3 + 1/2(3 - \gamma)u_2^2/u_1, \gamma u_2 u_3/u_1 - 1/2(\gamma - 1)u_2^3/u_1^2)^T, \end{aligned}$$

where ρ is the density, v is the velocity, E is the internal energy and γ is the ratio of specific heat. For the higher order derivatives the order of differentiation does not matter, i.e. $f_{m_l, k} = f_{m_k, l}$ and $f_{m_l, k, p} = f_{m_l, p, k} = f_{m_k, l, p} = f_{m_k, p, l} = f_{m_p, l, k} = f_{m_p, k, l}$ so only the first such permutation is expressed. One method to find the flux derivatives is to substitute the higher order derivatives into Eq. 7.

The first-order derivatives of the flux function f_1 are:

$$f_{1_1} = 0, \quad f_{1_2} = 1, \quad f_{1_3} = 0,$$

and the second- and third-order derivatives are:

$$f_{1_{l,k}} = 0, \quad l, k = 1, 2, 3,$$

$$f_{1_{l,k,p}} = 0, \quad l, k, p = 1, 2, 3.$$

The first-order derivatives of the flux function f_2 are:

$$f_{2_1} = \frac{1}{2}(\gamma - 3)\frac{u_2^2}{u_1^2}, \quad f_{2_2} = (3 - \gamma)\frac{u_2}{u_1}, \quad f_{2_3} = \gamma - 1,$$

the second-order derivatives are:

$$f_{2_{1,1}} = -\frac{u_2^2(\gamma-3)}{u_1^3}, \quad f_{2_{1,2}} = \frac{(\gamma-3)u_2}{u_1^2}, \quad f_{2_{1,3}} = 0,$$

$$f_{2_{2,2}} = \frac{(3-\gamma)}{u_1}, \quad f_{2_{2,3}} = 0, \quad f_{2_{3,3}} = 0,$$

and the third-order derivatives are:

$$f_{2_{1,1,1}} = 3\frac{u_2^2(\gamma-3)}{u_1^4}, \quad f_{2_{1,1,2}} = -2\frac{(\gamma-3)u_2}{u_1^3}, \quad f_{2_{1,1,3}} = 0,$$

$$f_{2_{1,2,2}} = \frac{(\gamma-3)}{u_1^2}, \quad f_{2_{1,2,3}} = 0, \quad f_{2_{1,3,3}} = 0,$$

$$f_{2_{2,2,2}} = 0, \quad f_{2_{2,2,3}} = 0, \quad f_{2_{3,3,3}} = 0.$$

The first-order derivatives of the flux function f_3 are:

$$f_{3_1} = -\frac{\gamma u_2 u_3}{u_1^2} + \frac{(\gamma-1)u_3^2}{u_1^3}, \quad f_{3_2} = \frac{\gamma u_3}{u_1} - \frac{3}{2}(\gamma - 1)\frac{u_2^2}{u_1^2}, \quad f_{3_3} = \frac{\gamma u_2}{u_1},$$

the second-order derivatives are:

$$f_{3_{1,1}} = 2\frac{\gamma u_2 u_3}{u_1^3} - 3\frac{(\gamma-1)u_3^2}{u_1^4}, \quad f_{3_{1,2}} = -\frac{\gamma u_3}{u_1^2} + 3\frac{(\gamma-1)u_2^2}{u_1^3}, \quad f_{3_{1,3}} = -\frac{\gamma u_2}{u_1^2},$$

$$f_{3_{2,2}} = -3\frac{(\gamma-1)u_2}{u_1^2}, \quad f_{3_{2,3}} = \frac{\gamma}{u_1}, \quad f_{3_{3,3}} = 0,$$

the third-order derivatives are:

$$f_{3_{1,1,1}} = 12\frac{u_2^3(\gamma-1)}{u_1^5} - 6\frac{\gamma u_2 u_3}{u_1^4}, \quad f_{3_{1,1,2}} = 2\frac{\gamma u_3}{u_1^3} - 9\frac{(\gamma-1)u_2^2}{u_1^4}, \quad f_{3_{1,1,3}} = 2\frac{\gamma u_2}{u_1^3},$$

$$f_{3_{1,2,2}} = 6(\gamma - 1)\frac{u_2}{u_1^3}, \quad f_{3_{1,2,3}} = -\frac{\gamma}{u_1^2}, \quad f_{3_{1,3,3}} = 0$$

$$f_{3_{2,2,2}} = -3\frac{\gamma-1}{u_1^2}, \quad f_{3_{2,2,3}} = 0, \quad f_{3_{3,3,3}} = 0.$$

Another method to find the flux derivatives is to use the product rule. As a preliminary we will show both the product and quotient rule for any derivative. First let $f(x, t) = g(x, t)h(x, t)$ then any derivative of f can be expressed as

$$\frac{\partial^{n+m} f}{\partial x^n \partial t^m} = \sum_{k=0}^n \sum_{l=0}^m \binom{n}{k} \binom{m}{l} \frac{\partial^{n+m-k-l} g}{\partial x^{n-k} \partial t^{m-l}} \frac{\partial^{k+l} h}{\partial x^k \partial t^l}$$

or solving for $\frac{\partial^{n+m}g}{\partial x^n \partial t^m}$ we can calculate any derivative of g

$$\frac{\partial^{n+m}g}{\partial x^n \partial t^m} = \frac{1}{h} \left[\frac{\partial^{n+m}f}{\partial x^n \partial t^m} - \sum_{k=0}^n \sum_{l=0}^m \binom{n}{k} \binom{m}{l} \frac{\partial^{n+m-k-l}g}{\partial x^{n-k} \partial t^{m-l}} \frac{\partial^{k+l}h}{\partial x^k \partial t^l} \text{ for } (k, l) \neq (0, 0) \right]$$

Now we can express any derivative of the fluxes

$$\begin{aligned} \frac{\partial^{n+m}f_1}{\partial x^n \partial t^m} &= \frac{\partial^{n+m}u_2}{\partial x^n \partial t^m} \\ \frac{\partial^{n+m}f_2}{\partial x^n \partial t^m} &= (\gamma - 1) \frac{\partial^{n+m}u_3}{\partial x^n \partial t^m} + \frac{3 - \gamma}{2} \sum_{k=0}^n \sum_{l=0}^m \binom{n}{k} \binom{m}{l} \frac{\partial^{n+m-k-l}u_2}{\partial x^{n-k} \partial t^{m-l}} \frac{\partial^{k+l}v}{\partial x^k \partial t^l} \\ \frac{\partial^{n+m}f_3}{\partial x^n \partial t^m} &= \sum_{k=0}^n \sum_{l=0}^m \binom{n}{k} \binom{m}{l} \left(\gamma \frac{\partial^{n+m-k-l}u_3}{\partial x^{n-k} \partial t^{m-l}} - \frac{\gamma - 1}{2} \frac{\partial^{n+m-k-l}u_2 v}{\partial x^{n-k} \partial t^{m-l}} \right) \frac{\partial^{k+l}v}{\partial x^k \partial t^l} \end{aligned} \quad (26)$$

We still need to express the derivatives of velocity as functions of flow variables.

$$\begin{aligned} \frac{\partial^{n+m}v}{\partial x^n \partial t^m} &= \frac{\partial^{n+m}}{\partial x^n \partial t^m} \left(\frac{u_2}{u_1} \right) = \\ &= \frac{1}{u_1} \left[\frac{\partial^{n+m}u_2}{\partial x^n \partial t^m} - \sum_{k=0}^n \sum_{l=0}^m \binom{n}{k} \binom{m}{l} \frac{\partial^{n+m-k-l}v}{\partial x^{n-k} \partial t^{m-l}} \frac{\partial^{k+l}u_1}{\partial x^k \partial t^l} \text{ for } (k, l) \neq (0, 0) \right] \end{aligned} \quad (27)$$

Since the left hand side is always the highest unknown derivative everything on the RHS is known. Equations (26) and (27) represent one possible formulation and is not guaranteed to be the most efficient. We used Eqs. (26) and (27) in our simulations.

To show higher order convergence for a non-linear equation we solve the acoustic equations. There are some problems when using the analytical solution because the Euler solver will capture the non-linearities present in the flow field while the ‘‘analytical’’ solution does not. This will lead to increasing errors in the analytical solution as Δx decreases. To mitigate the error, the perturbation was reduced to 10^{-6} . For this test case $p_\infty=1/\gamma$, $\rho_\infty=1$, $n=2$, and $l=4$ and the simulation time is $2.5 \frac{l}{a_\infty}$. The CFL number is almost constant throughout the domain and is equivalent to 0.8. The convergence rates are shown in table 3. From this table it can be seen that the computational cost associated with increasing the accuracy is approximately squared, e.g. if the order of accuracy is doubled then the CPU time will increase 4 times. As seen in fig. 8 using a higher order is typically more efficient than using more points.

Table 3.: Convergence rates of the numerical solutions of the convection equation, and the averaged, normalized time for case with different order of accuracy.

Desired Order	Actual Order	Normalized Time
2	2.00	1.00
4	3.97	2.84
8	7.48	12.40
12	11.96	32.30

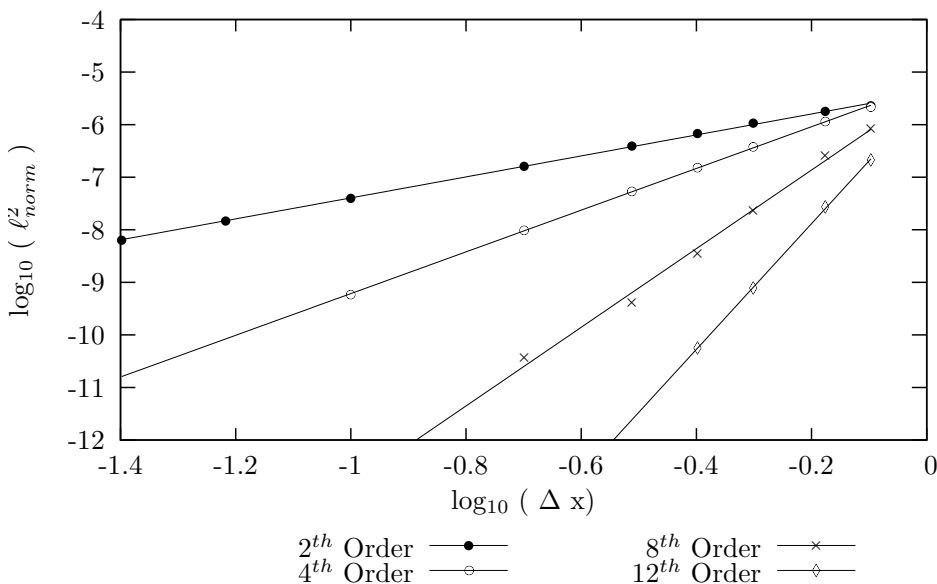


Figure 7.: The ℓ^2 norm of the numerical solutions of the Euler solver for solving the acoustic waves.

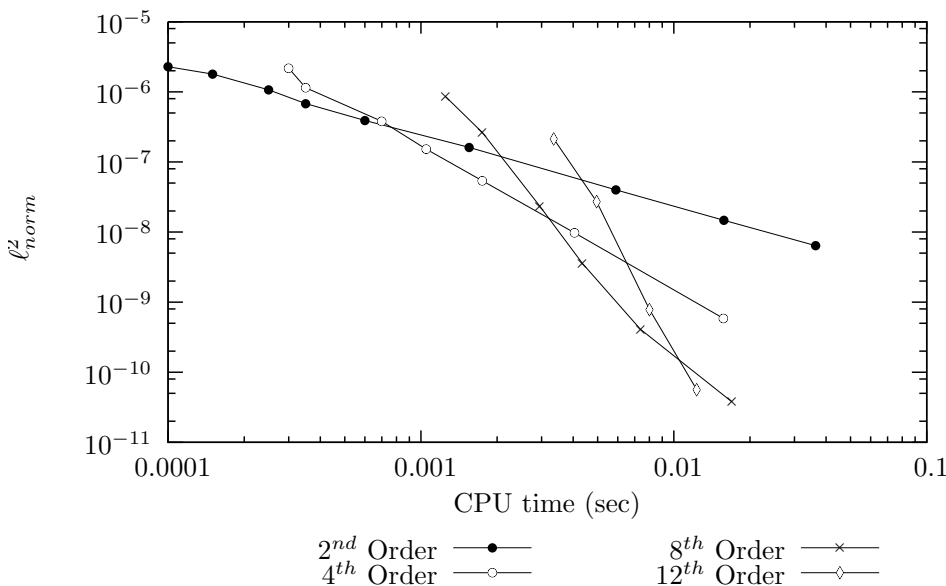


Figure 8.: The ℓ^2 norm versus the computational time for the solution to the non-linear Euler solver.

Next, we demonstrate the new high-order CESE method by examining numerical resolution for shocks and contact discontinuities. We will run two different test cases at various resolutions and compare the results with a converged solution obtained by using very fine mesh. The CESE and the fifth-order space third-order time monotonicity preserving (MP53) method (Suresh and Huynh (1997)). The CESE scheme is run at 4 different orders, 2, 4, 6, and 8th. The test cases chosen are Woodward’s blast wave problem and Shu and Osher’s problem. Woodward’s blast wave problem(Woodward and Colella (1984)) consists of two shock waves of different strengths heading towards each other with wall boundary conditions. The initial conditions are

$$(u, \rho, p) = \begin{cases} (0, 1, 10^3) & 0 < x < 0.1 \\ (0, 1, 10^{-2}) & 0.1 < x < 0.9 \\ (0, 1, 10^2) & 0.9 < x < 1.0 \end{cases}$$

$$0.0 < t < 0.038.$$

The second test case is Shu and Osher's problem (Shu and Osher (1989)), in which a Mach 3 shock moves to the right and collides with an entropy disturbance moving to the left. The boundary conditions are non-reflective and the initial conditions are

$$(u, \rho, p) = \begin{cases} (2.629369, 3.857143, 10.3333) & -1 < x < -0.8 \\ (0, 1 + 0.2 \sin(5\pi x), 1) & -0.8 < x < 1.0 \end{cases}$$

$$0.0 < t < 0.47.$$

For both simulations α in Eq. (20) varies by this equation.

$$\alpha = \min \left(\frac{1}{2} \left| \left(\frac{u_{m\bar{x}z+}^c}{u_{m\bar{x}z-}^c} + \frac{u_{m\bar{x}z-}^c}{u_{m\bar{x}z+}^c} \right) - 1 \right|, 1.0 \right).$$

Using this equation the value of α approaches zero as $u_{m\bar{x}z+}^c$ approaches $u_{m\bar{x}z-}^c$. β in Eq. (23) was set to 0.01.

Shown in Figures (9) and (10) the CESE results improve as the order of the solver increases. As the order of the solver increase it becomes more difficult to suppress the overshoot around discontinuities. This is seen in the 8th order Shu-Osher simulation. It was found that in order to suppress that overshoot the rest of the solution became more diffusive then the second order CESE solution. When evaluating the Shu-Osher simulations the MP scheme out performs the second order CESE scheme and compares favourably to the 4 and 6th order solutions. The 8th order CESE scheme does a better job then the MP except at the discontinuity where there is some overshoot. For the blastwave problem very few differences were seen between the different simulations. All solvers were able to resolve the shocks with one or two points. One difference is that in the 400 point case the MP scheme does a slightly better job when x is greater than 0.7 and less then 0.8. Also in the 800 point case the 4th order CESE scheme has more dissipation then the other schemes. This could be caused by switching to the minmod limiter too soon.

4. Concluding Remarks

In this paper, we extended Chang's fourth-order CESE method for one convection equation for solving a system of coupled hyperbolic PDE's with arbitrarily high-order convergence. Numerical results show that the extended algorithm can achieve higher-order convergence for both linear and non-linear hyperbolic PDEs. The shock-capturing capability of the new method was comparable to that of the original second-order CESE scheme as well as that of the fifth-order space third-order time monotonicity preserving scheme. Further development of the high-order CESE method can benefit from further development in several areas, including the effect of different limiters on the higher-order derivatives, and the effects of the boundary condition treatments and the source-term treatments for high-order accuracy.

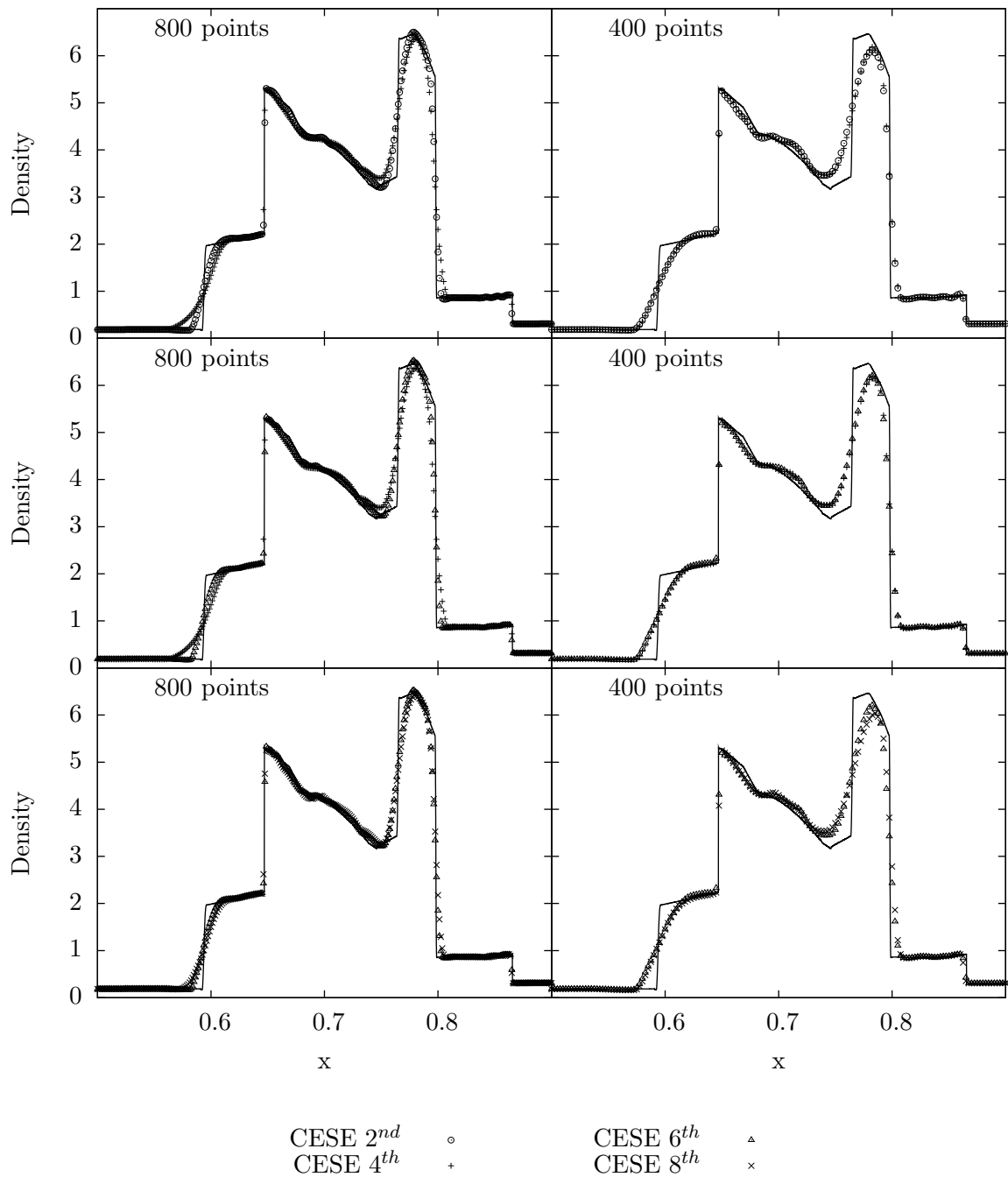


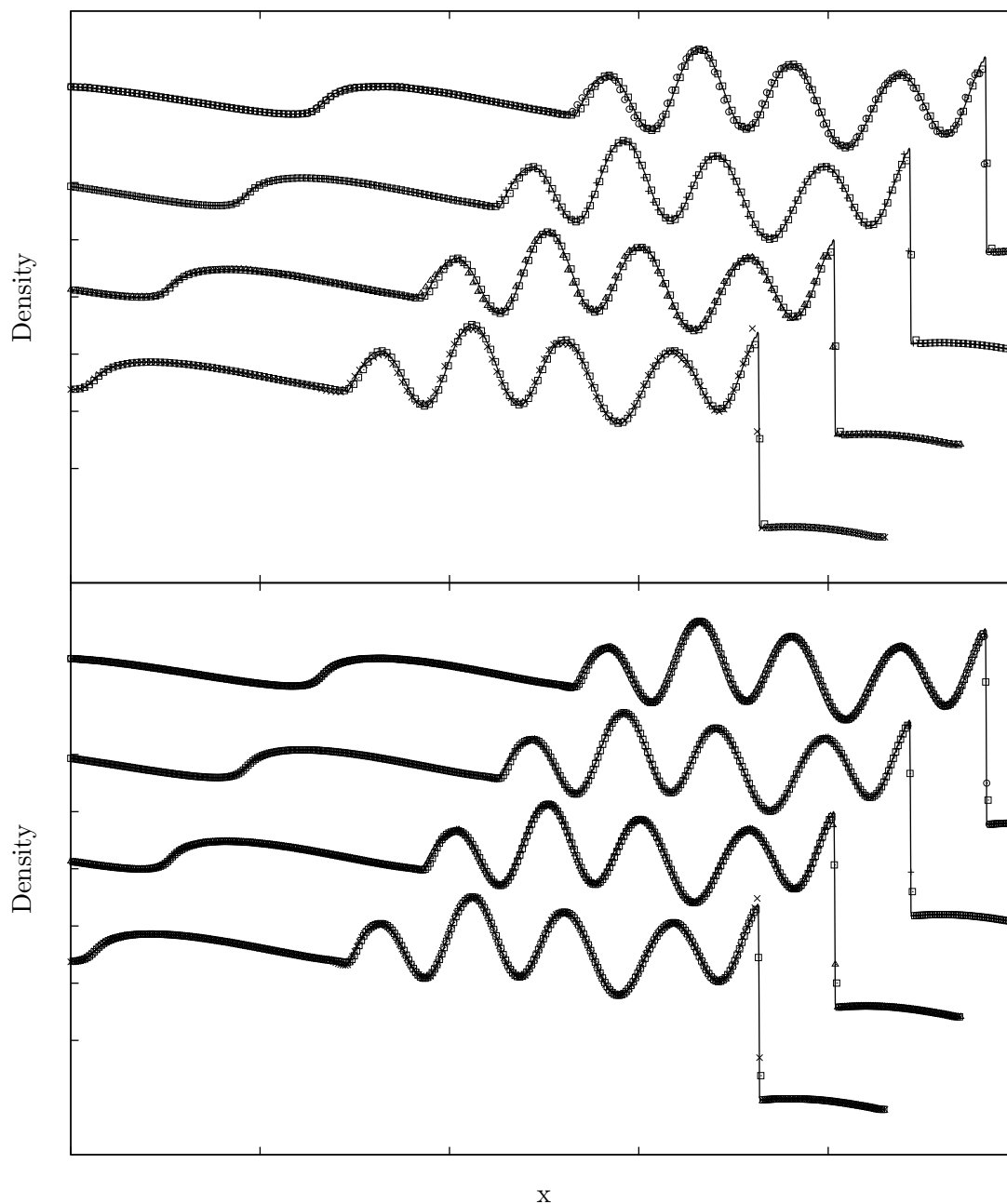
Figure 9.: Plots of the density profiles of the Woodward's blast wave problem. The converged simulation was done by using the second-order CESE with 20001 points. For better presentation, only a subset of the domain is shown in these plots.

5. Acknowledgments

The authors would like to thank Lord Cole for the MP53 solutions to Woodward's blast wave problem and Shu and Osher's test case.

References

- Chang, C., 2007. Three-Dimensional Navier-Stokes Calculations Using the Modified Space-Time CESE Method. *In: Cincinnati, Ohio.*
- Chang, S., 1995. The Method of Space-Time Conservation Element and Solution Element – A New Approach for Solving the Navier-Stokes and Euler Equations. *Journal of Computational Physics*, 119 (2), 295–324.
- Chang, S., 2010. A New Approach for Constructing Highly Stable High Order CESE Schemes. *In: Jan., AIAA-2010-543, 48th AIAA Aerospace Science Meeting, Orlando, FL.*
- Chang, S. and Wang, X., 2003. Multi-Dimensional Courant Number Insensitive CE/SE Euler Solvers for Applications Involving Highly Nonuniform Meshes. *In: 39th AIAA/ASME/SAE/ASEE Joint Propulsion Conference and Exhibit, Jul., Huntsville, Alabama.*
- Chen, Y., Yang, L., and Yu, S.J., 2011. Simulations of Waves in Elastic Solids of Cubic Symmetry by the Conservation Element and Solution Element Method. *Wave Motion*, 48 (1), 39–61.
- Roe, P.L., 1986. Characteristic-Based Schemes for the Euler Equations. *Annual Review of Fluid Mechanics*, 18 (1), 337–365.
- Shu, C. and Osher, S., 1989. Efficient implementation of essentially non-oscillatory shock capturing schemes II. *Journal of Computational Physics*, 83, 32–78.
- Suresh, A. and Huynh, H.T., 1997. Accurate Monotonicity-Preserving Schemes with Runge-Kutta Time Stepping. *Journal of Computational Physics*, 136 (1), 83–99.
- Venkatachari, B.S., *et al.*, 2008. Validation and verification of Courant number insensitive CE/SE method for transient viscous flow simulations. *Mathematics and Computers in Simulation*, 78 (5-6), 653–670.
- Woodward, P. and Colella, P., 1984. The numerical simulation of two-dimensional fluid flow with strong shocks. *Journal of Computational Physics*, 54, 115–173.
- Yang, L., Chen, Y., and Yu, S.J., 2011. Velocity-Stress Equations for Waves in Solids of Hexagonal Symmetry Solved by the Space-Time CESE Method. *ASME Journal of Vibration and Acoustics*, 133 (2), 021001.
- Zhang, M., *et al.*, 2006. Solving the MHD equations by the space-time conservation element and solution element method. *Journal of Computational Physics*, 214 (2), 599–617.
- Zhang, Z., *et al.*, 2000. The Space-Time CE/SE Method for Navier-Stokes Equations in Three Spatial Dimensions. *In: AIAA Paper 2000-2331, AIAA Fluid 2000 Conference, June 19-22, 2000, Denver, CO.*



MP53	□	CESE 4 th	+	CESE 8 th	×
CESE 2 nd	○	CESE 6 th	△		

Figure 10.: Plots of the calculated density profiles for Shu and Osher's problem. Each plot has a different spatial resolution. The converged simulation was done by using the second-order CESE scheme with 3201 points.